Available online at www.sciencedirect.com

ScienceDirect

Energy Procedia 124 (2017) 567–576

Energy Procedia

www.elsevier.com/locate/procedia

7th International Conference on Silicon Photovoltaics, SiliconPV 2017

Low temperature perovskite solar cells with an evaporated TiO_2 compact layer for perovskite silicon tandem solar cells

Alexander J. Bett[a,*], Patricia S. C. Schulze[a], Kristina Winkler[a], Jacopo Gasparetto[a], Paul F. Ndione[b], Martin Bivour[a], Andreas Hinsch[a], Markus Kohlstädt[a,c], Seunghun Lee[d], Simone Mastroianni[a], Laura E. Mundt[a], Markus Mundus[a], Christian Reichel[a], Armin Richter[a], Clemens Veit[a,c], Karl Wienands[e], Uli Würfel[a,c], Welmoed Veurman[a], Stefan W. Glunz[a,e], Martin Hermle[a], Jan Christoph Goldschmidt[a]

[a]*Fraunhofer Institute for Solar Energy Systems, Heidenhofstraße 2, 79110 Freiburg, Germany*
[b]*National Renewable Energy Laboratory, 15013 Denver West Parkway, Golden, CO 80401, USA*
[c]*Freiburg Materials Research Center FMF, University of Freiburg, Stefan-Meier-Straße 25, 79104 Freiburg, Germany*
[d]*Korea University, Anam Campus, Anam-dong 5-ga, Seongbuk-gu, Seoul, Korea*
[e]*Freiburg Center for Interactive Materials and Bioinspired Technologies (FIT), University of Freiburg, Georges-Köhler-Allee 105, 79110 Freiburg, Germany*

Abstract

Silicon-based tandem solar cells can overcome the efficiency limit of single junction silicon solar cells. Perovskite solar cells are particularly promising as a top cell in monolithic tandem devices due to their rapid development towards high efficiencies, a tunable band gap with a sharp optical absorption edge and a simple production process. In monolithic tandem devices, the perovskite solar cell is deposited directly on the silicon cell, requiring low-temperature processes (< 200°C) to maintain functionality of under-lying layers of the silicon cell in case of highly efficient silicon hetero-junction (SHJ) bottom solar cell. In this work, we present a complete low-temperature process for perovskite solar cells including a mesoporous titanium oxide (TiO_2) scaffold - a structure yielding the highest efficiencies for single-junction perovskite solar cells. We show that evaporation of the compact TiO_2 hole blocking layer and ultra-violet (UV) curing for the mesoporous TiO_2 layer allows for good performance, comparable to high-temperature (> 500°C) processes. With both manufacturing routes, we obtain short-circuit current densities (J_{SC}) of about 20 mA/cm², open-circuit voltages (V_{OC}) over 1 V, fill factors (*FF*) between 0.7 and 0.8 and efficiencies (η) of more than 15%. We further show that the evaporated TiO_2 layer is suitable for the application in tandem devices. The series resistance of the layer itself and the contact resistance to an indium doped tin oxide (ITO) interconnection

* Corresponding author. Tel.: +49-761-4588-5922
E-mail address: alexander.bett@ise.fraunhofer.de

Peer review by the scientific conference committee of SiliconPV 2017 under responsibility of PSE AG.
10.1016/j.egypro.2017.09.293

layer between the two sub-cells are low. In addition, the low parasitic absorption for wavelengths above the perovskite band gap allow a higher absorption in the silicon bottom solar cell, which is essential to achieve high tandem efficiencies.

Peer review by the scientific conference committee of SiliconPV 2017 under responsibility of PSE AG.

Keywords: Perovskite solar cell; low-temperature process; TiO_2/ITO resistance

1. Introduction

The efficiency of single junction silicon solar cells is limited to 29.4% [1]. The main loss mechanism is thermalization. The excess energy of photons with energies higher than the bandgap is transferred to the lattice and cannot be converted into electrical energy. To overcome this fundamental limit, tandem solar cells consisting of a silicon bottom solar cell and a top solar cell with a higher bandgap are investigated. A promising tandem partner for silicon is a perovskite top cell as the bandgap of the perovskite absorber can be adjusted for its use in tandem solar cells [2]. The two sub-cells in a tandem device can either be mechanically stacked (4-terminal device) or monolithically interconnected (2-terminal device). We aim for monolithic tandem solar cells, because (i) the integration of such cells in a module is potentially easier than in the case of 4-terminal devices and (ii) less intermediate layers for lateral current transport to the terminals are needed which typically cause parasitic absorption. To date, however, research groups reported more on mechanically stacked tandem solar cells [2–8] than on successful fabrication of monolithic tandem devices [8–12].

Since their emergence only few years ago, the power conversion efficiency of perovskite solar cells raised up to 22.1% [13]. Especially, the TiO_2-based mesoporous structure yielded high efficiencies [14–16]. In this structure the electron contact consists of a compact TiO_2 layer and a mesoporous TiO_2 scaffold that is infiltrated by the perovskite absorber. As reported in most of the publications about mesoporous perovskite solar cells, the electron contacts are typically fabricated by high-temperature processes (up to 500°C) such as spray pyrolysis deposition for the compact layer and sintering of the mesoporous layer [14–17]. However, in tandem solar cells a low-temperature process (below 200°C) can be beneficial. In particular, when using silicon hetero-junction (SHJ) bottom solar cells, allowing for high voltage and overall high efficiency [18,19], a low-temperature process is required in order to avoid the degradation of the SHJ solar cell [19,20]. Not only for SHJ solar cells but also for other silicon bottom solar cells, a low-temperature process is beneficial when indium-doped tin oxide (ITO) is used as a recombination layer since the interface between ITO and silicon might not withstand high temperatures [21]. Several research groups reported on the low-temperature fabrication of a compact TiO_2 layer using spin coating [22,23], atomic layer deposition (ALD) [24,25] or sputtering [7]. To the best of our knowledge only one group presented a complete low-temperature process for TiO_2-based mesoporous perovskite solar cells. Di Giacomo et al. used ALD for the compact layer and a UV treatment of the mesoporous TiO_2 [26].

Figure 1 represents a possible structure of a perovskite silicon tandem device with a SHJ bottom solar cell and a low-temperature processed mesoporous perovskite top solar cell. In this case an ITO interconnection layer is situated between the amorphous silicon (a-Si) hole conductor of the bottom solar cell and the TiO_2 electron contact of the top solar cell.

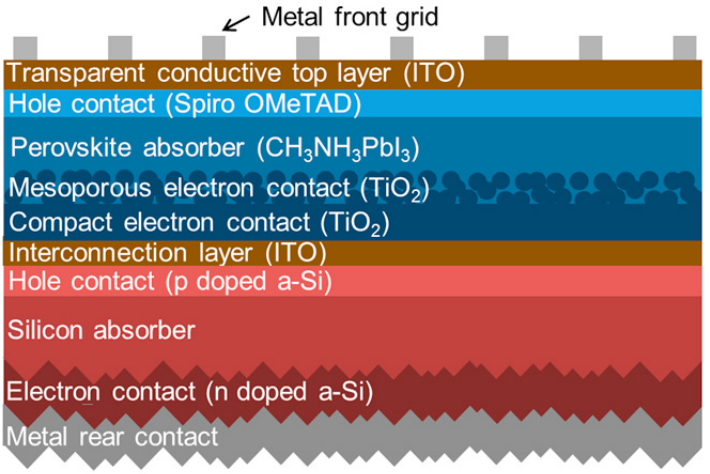

Fig. 1. Schematic sketch of a tandem solar cell consisting of a SHJ bottom solar cell and a mesoporous perovskite top solar cell. In such a structure the TiO_2 must exhibit low resistance in combination with the interconnecting ITO and should not absorb light useful for the silicon bottom solar cell.

In this paper, we discuss a compact TiO_2 layer deposited by electron beam evaporation allowing for low substrate temperatures as hole blocking layer for perovskite solar cells. First, we demonstrate that the resistance of a layer stack consisting of ITO and evaporated TiO_2 as well as the absorption coefficient of the evaporated TiO_2 is sufficiently low. Hence, this layer is a promising candidate for the use in a perovskite silicon tandem solar cell with a SHJ bottom solar cell. In the second step we show that the evaporated TiO_2 layer works as a hole blocking layer in perovskite solar cells. Together with a mesoporous TiO_2 treated by UV irradiation instead of high-temperature sintering we are able to produce low-temperature mesoporous perovskite solar cells. Both required low-temperature process steps have been optimized. In this work we focus on the evaporation of the compact TiO_2. Optimization of the UV treatment of the mesoporous layer can be found elsewhere [21]. We show that the conventional high-temperature and the new, optimized low-temperature process route lead to comparable results.

2. Experimental methods

2.1. Fabrication of samples to determine resistivity of ITO/TiO2 interface and TIO2 layer

To evaluate the contribution of the evaporated TiO_2 layer to the series resistance in a tandem solar cell (pass resistance through the TiO_2 layer itself and contact resistance to the under-lying ITO layer), conductivity samples were fabricated on silicon wafers (n-type, 1 Ω cm, float zone, thickness 200 µm). To achieve good conductivity to subsequent layers, the wafers received a phosphorus diffusion on both sides with a sheet resistance of approximately 50 Ω/sq. The rear side was metallized by subsequently evaporating 50 nm of titanium, 50 nm of palladium and 1000 nm of silver (Ti/Pd/Ag). Subsequently, a 20 nm thick indium-doped tin oxide (ITO) layer was sputtered at the front side in an Oxford instruments system. Then, a 20 nm thick TiO_2 layer was evaporated on the front side by electron beam evaporation in an evaporation tool (Pfeiffer PLS 570) equipped with a voltage electron gun (Telemark Model 267). The pressure during evaporation was 10^{-4} mbar. The substrate temperature was around 20°C and the evaporation rate was 1 nm/s controlled by an oscillating crystal. A second 20 nm thick ITO layer was sputtered on top of the TiO_2. Thus, the TiO_2 layer is sandwiched between two ITO layers. In this configuration, the overall resistance is dominated by the contact resistance between TiO_2 and ITO and the resistance for the vertical current flow through the TiO_2. These are also the two contributions which are relevant in a final tandem device, in regard to the TiO_2. As reference, samples without TiO_2 (ITO layer of double thickness (40 nm)) were fabricated. In a final

step, the front side was also metallized with Ti/Pd/Ag and samples were cut into pieces with a size of 2 x 2 cm^2 by lasering or sawing using a dicing saw.

2.2. Perovskite solar cell fabrication

Perovskite solar cells were fabricated on fluorine-doped tin oxide (FTO) coated glass substrates. The FTO was structured according to the cell layout by etching with hydrochloric acid and zinc powder in order to avoid short-circuiting the solar cell. After cleaning the substrates, a compact TiO_2 hole blocking layer was evaporated as described in section 2.1. We investigated different layer thicknesses of 10 nm, 20 nm, 30 nm and 50 nm. Afterwards, a mesoporous TiO_2 scaffold was spin coated from a solution containing a commercial TiO_2 paste, ethanol and terpineol. The samples were then exposed to UV irradiation for 120 min and 200 min, respectively. For comparison, high-temperature solar cells were fabricated by spray deposition of the compact TiO_2 layer at 470°C and sintering of the mesoporous layer at 525°C. The perovskite absorber material, methylammonium lead triiodide ($CH_3NH_3PbI_3$), was spin-coated in a nitrogen filled glovebox from a stoichiometric solution of methylammonium iodide (MAI) and lead iodide (PbI_2) in dimethylsulfoxide (DMSO). Toluene was added as an antisolvent 5 s prior to the end of the spin coating process and afterwards the substrates were annealed at 100°C for 60 min. For the hole conductor, doped 2,2',7,7'-Tetrakis-(*N*,*N*-di-4-methoxyphenylamino)-9,9'-spirobifluorene (Spiro-OMeTAD) [17], was spin-coated, still in the glovebox. Finally, gold contacts were thermally evaporated through a shadow mask to define three cells on each substrate. More details about the utilized materials and process steps can be found elsewhere [21].

A schematic sketch of the structure is represented in Fig. 2a. Fig. 2b shows a scanning electron microscope (SEM) picture of a perovskite solar cell fabricated by the low-temperature process. The process sequences for the manufacturing of the low-temperature solar cells and the high-temperature reference cells are shown in Fig. 2c.

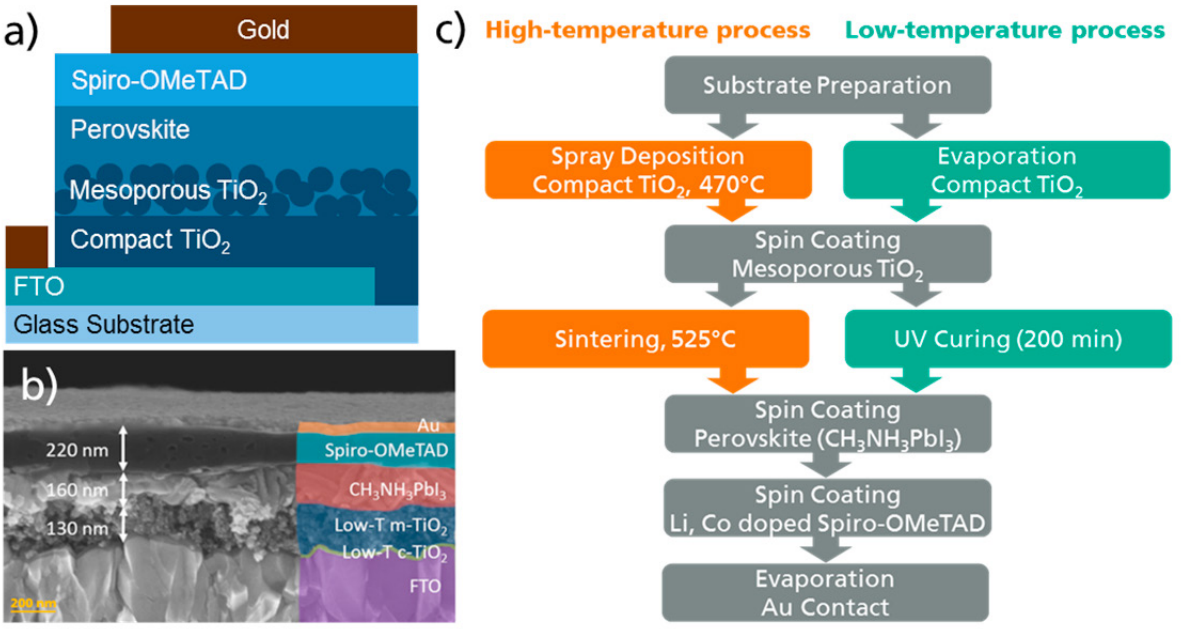

Fig. 2. (a) Sketch of a perovskite solar cell. (b) SEM picture of a perovskite solar cell fabricated by the low-temperature process. (c) Process sequence for fabrication of high- and low-temperature perovskite solar cells.

2.3. Characterization methods

Resistance measurements were conducted using a Keithley 2651A source meter recording the current-voltage characteristics. Resistance values were afterwards determined by a linear least square fit in a current density range between 15 mA/cm² and 30 mA/cm².

The optical functions of the TiO_2 films (evaporated on silicon) were determined using spectroscopical ellipsometry (J.A.Woollam M-2000 ellipsometer). The refractive index and extinction coefficient were extracted by fitting the ellipsometric data (Psi, Delta) with a Tauc-Lorentz dispersion model.

Current-Voltage (IV) characteristics of perovskite solar cells were measured using a sun simulator consisting of a xenon short arc lamp (Wacom, 1000 W) and a source meter (Keithley 2651A). Light intensity was calibrated using a silicon reference solar cell to have an illumination of 1 sun intensity according to the air mass 1.5 global (AM1.5g) spectrum. Every solar cell was first measured in reverse scan direction (from 1.2 V to -0.1 V) and afterwards in forward scan direction (from -0.1 V to 1.2 V). The scan speed was 43 mV/s. A shadow mask defined an active area of 0.16 cm² during the measurement.

3. Results and discussion

3.1. Characterization of the evaporated TiO_2 layer

For using evaporated TiO_2 layer in a tandem device as represented in Fig. 1, there are two main requirements: First, the resistance for the vertical current flow through the TiO_2 and the contact resistance between TiO_2 and ITO have to be as low as possible in order to keep the series resistance of the tandem solar cell low. Second, the layer should not parasitically absorb in the spectral range that is used by the silicon bottom solar cell.

The results of the resistance measurements are represented in Fig. 3a together with the investigated structures. The reference samples containing a 40 nm thick ITO layer without TiO_2 show a very small resistance of $(0.027 \pm 0.002)\ \Omega\ cm^2$ which is basically the resistance contribution of the silicon wafer and shows that there is no significant resistance contribution of the ITO layer and the metal contacts. The samples with a 20 nm thick evaporated TiO_2 layer sandwiched between two 20 nm thick ITO layers have a resistance of $(0.46 \pm 0.17)\ \Omega\ cm^2$. As the series resistance of perovskite solar cells is typically between 3 Ω cm² and 10 Ω cm² [8,15,27–31], it represents a reasonable value. Assuming a current density of 20 mA/cm² which is a reasonable value for good perovskite solar cells [2,15,32–34], a voltage of around 9 mV is lost when using an ITO/TiO_2 interconnection between the two sub-cells. This value could be considered as an upper limit for what should be expected in a tandem solar cell, as in our test samples the ITO/TiO_2 interface occurs tow times, while it will only occur once in a tandem solar cell. On the other hand, pin holes might be present in the TiO_2 layer, reducing the resistance in comparison to a pin hole free layer.

Fig. 3b shows the extinction coefficient k of the evaporated TiO_2 layer. It is zero for wavelengths longer than 400 nm. Thus, the evaporated TiO_2 only absorbs in the UV range of the spectrum. However, in this part of the spectrum, the perovskite is strongly absorbing [35,36] and thus, no light will reach the underlying TiO_2 layer in that spectral region and no parasitic absorption of the TiO_2 will degrade the performance of the tandem solar cell.

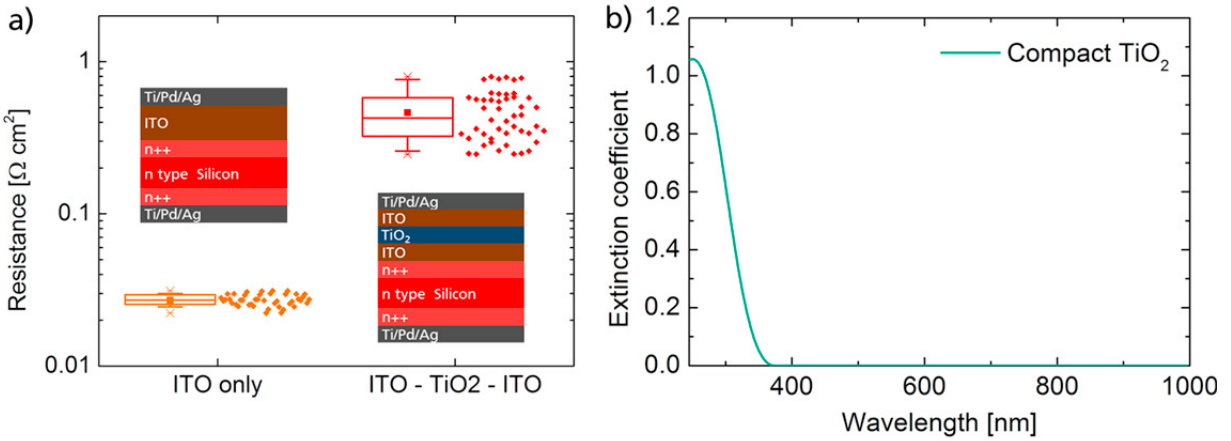

Fig. 3. (a) Resistance of an ITO-TiO_2-ITO stack compared to an ITO-ITO reference. Inset sketches show the structure of the investigated samples. (b) Extinction coefficient of TiO_2 determined by spectral ellipsometry. The investigated TiO_2 fulfills both requirements for the use in a tandem configuration: low resistivity in combination with ITO and no parasitic absorption in the spectral range useful for the silicon bottom solar cell.

3.2. Perovskite solar cells

To test our TiO_2 layers at device level, four groups of solar cells with different thicknesses (10 nm, 20 nm, 30 nm and 50 nm) of evaporated TiO_2 were fabricated. In this batch, the samples were kept under UV irradiation for 120 min after spin-coating the mesoporous TiO_2 scaffold. Fig. 4 shows short-circuit current density J_{SC}, open-circuit voltage V_{OC}, fill factor *FF*, and efficiency obtained from forward and reverse scan direction in dependence of the layer thickness. For a 50 nm thick compact TiO_2 only very few cells could be measured and their efficiency was below 0.5%. Thus, this group of cells is not represented in the graphs. For all working solar cells a hysteresis effect is present, i.e. a difference between current-voltage curves obtained from forward and reverse scan direction. This effect might be explained by interplay between surface recombination and ion migration within the perovskite absorber [37]. Following this argumentation, by improving the quality of the selective contacts the hysteresis can be reduced. With a compact layer thickness of 10 min, some cells achieved good efficiencies of up to 13.39% and 16.71%, measured in forward and reverse scan direction, respectively. But the spread is very high and there are also cells with very poor efficiency. On average, the hysteresis is most pronounced for this group of solar cells. Two cells even showed a maximum of the current near the maximum power point in the reverse scan direction resulting in unrealistic FF of nearly 100%. Thus, an only 10 nm thick compact TiO_2 layer seems to be associated with a high surface recombination. One explanation is that with such thin layers, defects like pinholes might be present. Alternatively, capacitive effects that do not involve ion-migration and surface defects could be the source of the hysteresis [38]. However, it is not clear which mechanism would explain the observed dependence on the TiO_2 thickness following this line of thought. Considering the V_{OC}, some cells with 10 nm of evaporated TiO_2 only reach values below 0.9 V, whereas the spread for 20 nm and 30 nm is much smaller reaching open-circuit voltages of around 1 V. Generally, the results for evaporated TiO_2 layers of 20 nm and 30 nm are comparable. As the mean value and the median of efficiency are slightly higher for the 20 nm thick layer, we used this thickness for further experiments.

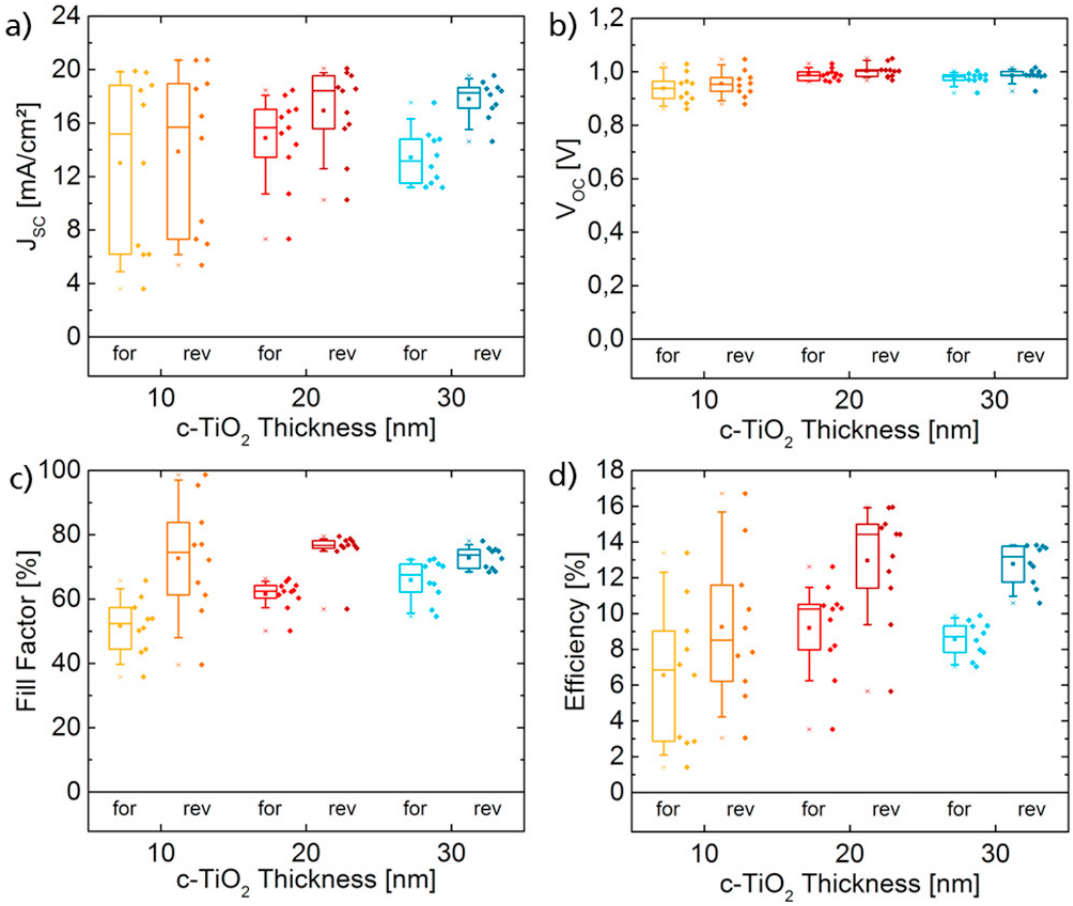

Fig. 4. (a) Short-circuit current density (J_{SC}), (b) open-circuit voltage (V_{OC}), (c) fill factor and (d) efficiency of perovskite solar cells fabricated by the low-temperature process (UV curing time 120 min) as a function of the evaporated compact TiO_2 (c-TiO_2) layer thickness. For each thickness, data from forward (for) and reverse (rev) scan direction are shown. 50% of the data points are within the boxes, 80% within the whiskers. The horizontal line and the point in the boxes represent the median and the mean value, respectively. In the mean, the best results were achieved with the cells having a 20 nm thick compact TiO_2 layer.

In a following solar cell batch we varied the UV irradiation time of the mesoporous TiO_2 scaffold. Details concerning this experiment can be found elsewhere [21]. By increasing the UV curing time to 200 min, solar cell performances get slightly better and the hysteresis is less pronounced. Fig. 5 represents a comparison of the best solar cells fabricated by the conventional high-temperature process (spray pyrolysis deposition of the compact TiO_2 and sintering of the mesoporous TiO_2) and the optimized low-temperature process (evaporation of a 20 nm thick compact TiO_2 layer and UV irradiation of the mesoporous TiO_2 for 200 min). With the low-temperature process we achieve similar values compared to the conventional high-temperature route. J_{sc} of around 20 mA/cm², V_{oc} over 1 V, and *FF* higher than 70% lead to efficiencies of around 15% in both cases. The mean efficiency of 12 cells produced by the optimized low-temperature process is 12.53% and 15.15% determined from forward and reverse scan directions, respectively. Thus, device performance of solar cells fabricated by our optimized low-temperature process is comparable to the results from the low-temperature process using ALD for the compact TiO_2 presented by Di Giacomo et al. [26].

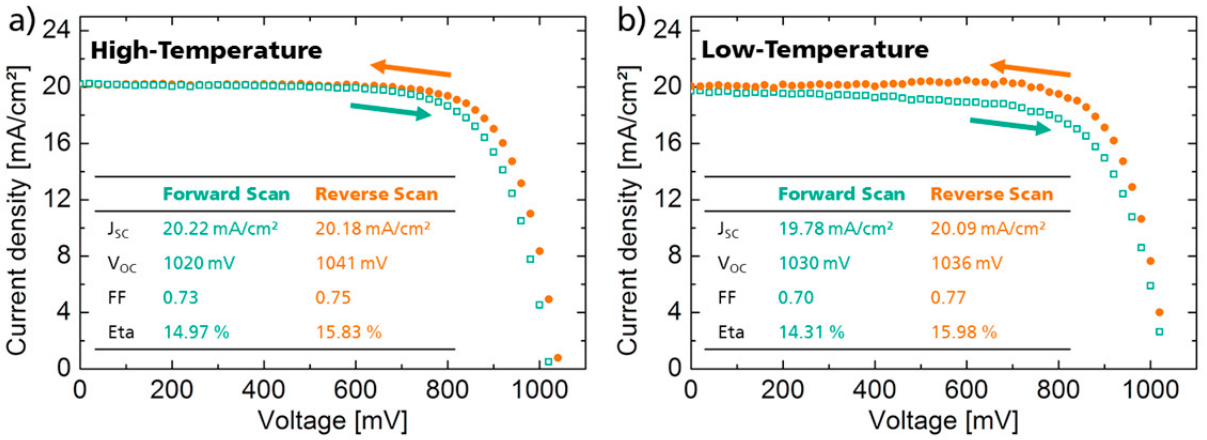

Fig. 5. IV curves of the best solar cells produced by the (a) high-temperature and (b) low-temperature process. Inset tables show the solar cell parameters. With both processes efficiencies of over 15% could be achieved.

4. Conclusion and outlook

We have shown that a low-temperature evaporated TiO_2 layer is suitable for the use as a hole blocking layer for the perovskite solar cell in perovskite silicon tandem devices using a SHJ bottom solar cell and an ITO interconnection layer. The sum of the contact resistance between ITO and TiO_2 and the pass resistance of the TiO_2 layer itself is below 0.5 Ωcm² and the extinction coefficient of the TiO_2 is zero in the spectral range useful for the silicon bottom solar cell. We further tested the evaporated TiO_2 as an electron contact in perovskite solar cells. With an optimized thickness of 20 nm and a low-temperature UV treatment of a mesoporous TiO_2 scaffold we achieved efficiencies up to over 15% which is comparable to the performance of solar cells fabricated by a conventional high-temperature process (spray pyrolysis deposition of the compact TiO_2 and sintering of the scaffold).

To realize perovskite silicon tandem solar cells we are currently investigating semitransparent perovskite solar cells. The full-area gold contact of the perovskite solar cell will be replaced by a contact grid. As the conductivity of Spiro-OMeTAD is too low to transport charge carriers laterally to the contact fingers, an additional transparent and conductive layer is needed.

Acknowledgements

This work was partially funded by the German Federal Ministry for Economic Affairs and Energy under contract number 0324037A (PersiST). A. J. Bett gratefully acknowledges scholarship support from the Deutsche Bundesstiftung Umwelt (DBU). The authors would like to thank Felix Schätzle, Karin Zimmermann, Harald Steidl, Markus Wichmann, Jutta Zielonka and Christian Harmel for processing support.

References

[1] A. Richter, M. Hermle and S. W. Glunz, “Reassessment of the limiting efficiency for crystalline silicon solar cells”, IEEE J. Photovoltaics, 3(4), 1184–1191 (2013).

[2] D. P. McMeekin, G. Sadoughi, W. Rehman, G. E. Eperon, M. Saliba, M. T. Horantner et al., “A mixed-cation lead mixed-halide perovskite absorber for tandem solar cells”, Science, 351(6269), 151–155 (2016).

[3] C. D. Bailie, M. G. Christoforo, J. P. Mailoa, A. R. Bowring, E. L. Unger, W. H. Nguyen et al., “Semi-transparent perovskite solar cells for tandems with silicon and CIGS”, Energ. Environ. Sci., 8(3), 956–963 (2015).

[4] K. A. Bush, C. D. Bailie, Y. Chen, A. R. Bowring, W. Wang, W. Ma et al., "Thermal and Environmental Stability of Semi-Transparent Perovskite Solar Cells for Tandems Enabled by a Solution-Processed Nanoparticle Buffer Layer and Sputtered ITO Electrode", Adv. Mat., 28(20), 3937–3943 (2016).
[5] P. Löper, S.-J. Moon, Martin de Nicolas, Silvia, B. Niesen, M. Ledinsky, S. Nicolay et al., "Organic-inorganic halide perovskite/crystalline silicon four-terminal tandem solar cells", Phys. Chem. Chem. Phys., 17(3), 1619–1629 (2015).
[6] F. Lang, M. A. Gluba, S. Albrecht, J. Rappich, L. Korte, B. Rech et al., "Perovskite Solar Cells with Large-Area CVD-Graphene for Tandem Solar Cells", J. Phys. Chem. Lett., 6(14), 2745–2750 (2015).
[7] J. Werner, G. Dubuis, A. Walter, P. Löper, S.-J. Moon, S. Nicolay et al., "Sputtered rear electrode with broadband transparency for perovskite solar cells", Sol. Energ. Mat. Sol. C., 141, 407–413 (2015).
[8] J. Werner, L. Barraud, A. Walter, M. Bräuninger, F. Sahli, D. Sacchetto et al., "Efficient Near-Infrared-Transparent Perovskite Solar Cells Enabling Direct Comparison of 4-Terminal and Monolithic Perovskite/Silicon Tandem Cells", ACS Energ. Lett., 1(2), 474–480 (2016).
[9] J. Werner, C.-H. Weng, A. Walter, L. Fesquet, J. P. Seif, S. de Wolf et al., "Efficient Monolithic Perovskite/Silicon Tandem Solar Cell With Cell Area 1 cm^2", J. Phys. Chem. Lett., 7(1), 161–166 (2016).
[10] J. P. Mailoa, C. D. Bailie, E. C. Johlin, E. T. Hoke, A. J. Akey, W. H. Nguyen et al., "A 2-terminal perovskite/silicon multijunction solar cell enabled by a silicon tunnel junction", Appl. Phys. Lett., 106(12), 121105 (2015).
[11] S. Albrecht, M. Saliba, J. P. Correa Baena, F. Lang, L. Kegelmann, M. Mews et al., "Monolithic Perovskite/Silicon-Heterojunction Tandem Solar Cells Processed at Low Temperature", Energ. Environ. Sci., 9(1), 81–88 (2016).
[12] K. A. Bush, A. F. Palmstrom, Z. J. Yu, M. Boccard, R. Cheacharoen, J. P. Mailoa et al., "23.6%-efficient monolithic perovskite/silicon tandem solar cells with improved stability", Nature Energy, 2, 17009 (2017).
[13] NREL, "Best Research-Cell Efficiencies", 2017. http://www.nrel.gov/ncpv/images/efficiency_chart.jpg.
[14] W. S. Yang, J. H. Noh, N. J. Jeon, Y. C. Kim, S. Ryu, J. Seo et al., "High-performance photovoltaic perovskite layers fabricated through intramolecular exchange", Science, 348(6240), 1234–1237 (2015).
[15] J.-P. Correa-Baena, M. Anaya, G. Lozano, W. Tress, K. Domanski, M. Saliba et al., "Unbroken Perovskite: Interplay of Morphology, Electro-optical Properties, and Ionic Movement", Adv. Mater., 28(25), 5031–5037 (2016).
[16] M. Saliba, T. Matsui, J.-Y. Seo, K. Domanski, J.-P. Correa-Baena, M. K. Nazeeruddin et al., "Cesium-containing triple cation perovskite solar cells: improved stability, reproducibility and high efficiency", Energ. Environ. Sci., 9(6), 1989–1997 (2016).
[17] J. Burschka, N. Pellet, S.-J. Moon, R. Humphry-Baker, P. Gao, M. K. Nazeeruddin et al., "Sequential deposition as a route to high-performance perovskite-sensitized solar cells", Nature, 499(7458), 316–319 (2013).
[18] K. Masuko, M. Shigematsu, T. Hashiguchi, D. Fujishima, M. Kai, N. Yoshimura et al., "Achievement of More Than 25% Conversion Efficiency With Crystalline Silicon Heterojunction Solar Cell", IEE J. Photovoltaics, 4(6), 1433–1435 (2014).
[19] S. de Wolf, A. Descoeudres, Z. C. Holman and C. Ballif, "High-efficiency Silicon Heterojunction Solar Cells: A Review", Green, 2(1), 7–24 (2012).
[20] S. de Wolf and M. Kondo, "Nature of doped a-Si: H/c-Si interface recombination", J. Appl. Phys., 105(10), 103707 (2009).
[21] P. S. C. Schulze, A. J. Bett, K. Winkler, A. Hinsch, S. Lee, S. Mastroianni, L. E. Mundt, M. Mundus, U. Würfel, S. W. Glunz, M. Hermle, J. C. Goldschmidt, "Low-Temperature Process for Perovskite Solar Cells with a Mesoporous TiO_2 Scaffold", submitted (2017).
[22] Y. Hou, H. Zhang, W. Chen, S. Chen, Quiroz, Cesar Omar Ramirez, H. Azimi et al., "Inverted, Environmentally Stable Perovskite Solar Cell with a Novel Low-Cost and Water-Free PEDOT Hole-Extraction Layer", Adv. Energ. Mat., 5(15), 1500543 (2015).
[23] M. Liu, M. B. Johnston and H. J. Snaith, "Efficient planar heterojunction perovskite solar cells by vapour deposition", Nature, 501(7467), 395–398 (2013).
[24] B. J. Kim, D. H. Kim, Y.-Y. Lee, H.-W. Shin, G. S. Han, J. S. Hong et al., "Highly efficient and bending durable perovskite solar cells: Toward a wearable power source", Energ. Enviro. Sci., 8(3), 916–921 (2015).
[25] Y. Wu, X. Yang, H. Chen, K. Zhang, C. Qin, J. Liu et al., "Highly compact TiO_2 layer for efficient hole-blocking in perovskite solar cells", Appl. Phys. Express, 7(5), 52301 (2014).
[26] F. Di Giacomo, V. Zardetto, G. Lucarelli, L. Cinà, A. Di Carlo, M. Creatore et al., "Mesoporous perovskite solar cells and the role of nanoscale compact layers for remarkable all-round high efficiency under both indoor and outdoor illumination", Nano Energy, 30, 460–469 (2016).
[27] F. Hao, C. C. Stoumpos, D. H. Cao, Chang, Robert P. H. and M. G. Kanatzidis, "Lead-free solid-state organic-inorganic halide perovskite solar cells", Nat. Photonics, 8(6), 489–494 (2014).
[28] J. H. Kim, P.-W. Liang, S. T. Williams, N. Cho, C.-C. Chueh, M. S. Glaz et al., "High-performance and environmentally stable planar heterojunction perovskite solar cells based on a solution-processed copper-doped nickel oxide hole-transporting layer", Adv. Mat. (Deerfield Beach, Fla.), 27(4), 695–701 (2015).
[29] J.-W. Lee, D.-H. Kim, H.-S. Kim, S.-W. Seo, S. M. Cho and N.-G. Park, "Formamidinium and Cesium Hybridization for Photo- and Moisture-Stable Perovskite Solar Cell", Adv. Energ. Mat., 5(20), 1501310 (2015).
[30] J. Liu, Y. Wu, C. Qin, X. Yang, T. Yasuda, A. Islam et al., "A dopant-free hole-transporting material for efficient and stable perovskite solar cells", Energ. Environ. Sci., 7(9), 2963 (2014).
[31] E. H. Anaraki, A. Kermanpur, L. Steier, K. Domanski, T. Matsui, W. Tress et al., "Highly efficient and stable planar perovskite solar cells by solution-processed tin oxide", Energ. Environ. Sci., 9(10), 3128–3134 (2016).

[32] J. P. Correa Baena, L. Steier, W. Tress, M. Saliba, S. Neutzner, T. Matsui et al., "Highly efficient planar perovskite solar cells through band alignment engineering", Energ. Environ. Sci., 8(10), 2928–2934 (2015).
[33] M. Saliba, T. Matsui, K. Domanski, J.-Y. Seo, A. Ummadisingu, S. M. Zakeeruddin et al., "Incorporation of rubidium cations into perovskite solar cells improves photovoltaic performance", Science, 354(6309), 206–209 (2016).
[34] H. Zhou, Q. Chen, G. Li, S. Luo, T.-b. Song, H.-S. Duan et al., "Photovoltaics. Interface engineering of highly efficient perovskite solar cells", Science (New York, N.Y.), 345(6196), 542–546 (2014).
[35] C.-W. Chen, S.-Y. Hsiao, C.-Y. Chen, H.-W. Kang, Z.-Y. Huang and H.-W. Lin, "Optical properties of organometal halide perovskite thin films and general device structure design rules for perovskite single and tandem solar cells", J. Mat. Chem. A, 3(17), 9152–9159 (2015).
[36] X. Ziang, L. Shifeng, Q. Laixiang, P. Shuping, W. Wei, Y. Yu et al., "Refractive index and extinction coefficient of $CH_3NH_3PbI_3$ studied by spectroscopic ellipsometry", Opt. Mat. Express, 5(1), 29 (2015).
[37] C. Eames, J. M. Frost, P. R. F. Barnes, B. C. O'Regan, A. Walsh and M. S. Islam, "Ionic transport in hybrid lead iodide perovskite solar cells", Nat. Comm, 6, 7497 (2015).
[38] N. K. Elumalai and A. Uddin, "Hysteresis in organic-inorganic hybrid perovskite solar cells", Sol. Energ. Mat. Sol. C, 157, 476-509 (2016).